ACCOUNTS
of chemical research

# High Frequency Dynamic Nuclear Polarization

QING ZHE NI,[†,‡] EUGENIO DAVISO,[†,‡,∥] THACH V. CAN,[†,‡]
EVGENY MARKHASIN,[†,‡] SUDHEER K. JAWLA,[§]
TIMOTHY M. SWAGER,[‡] RICHARD J. TEMKIN,[§]
JUDITH HERZFELD,[∥] AND ROBERT G. GRIFFIN*[,†,‡]

[†]*Francis Bitter Magnet Laboratory,* [‡]*Department of Chemistry, and* [§]*Plasma Science and Fusion Center, Massachusetts Institute of Technology, Cambridge, Massachusetts 02139, United States, and* [∥]*Department of Chemistry, Brandeis University, Waltham, Massachusetts 02454, United States*

RECEIVED ON DECEMBER 21, 2012

## CONSPECTUS

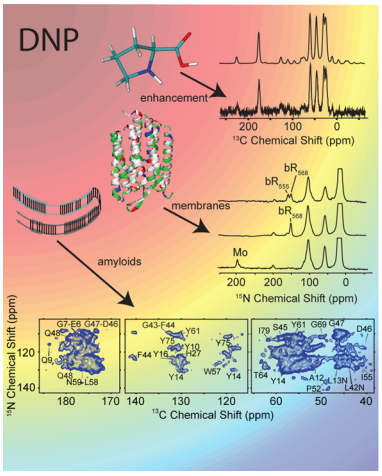


During the three decades 1980−2010, magic angle spinning (MAS) NMR developed into the method of choice to examine many chemical, physical, and biological problems. In particular, a variety of dipolar recoupling methods to measure distances and torsion angles can now constrain molecular structures to high resolution. However, applications are often limited by the low sensitivity of the experiments, due in large part to the necessity of observing spectra of low-$\gamma$ nuclei such as the I = 1/2 species $^{13}$C or $^{15}$N. The difficulty is still greater when quadrupolar nuclei, such as $^{17}$O or $^{27}$Al, are involved. This problem has stimulated efforts to increase the sensitivity of MAS experiments. A particularly powerful approach is dynamic nuclear polarization (DNP) which takes advantage of the higher equilibrium polarization of electrons (which conventionally manifests in the great sensitivity advantage of EPR over NMR). In DNP, the sample is doped with a stable paramagnetic polarizing agent and irradiated with microwaves to transfer the high polarization in the electron spin reservoir to the nuclei of interest. The idea was first explored by Overhauser and Slichter in 1953. However, these experiments were carried out on static samples, at magnetic fields that are low by current standards. To be implemented in contemporary MAS NMR experiments, DNP requires microwave sources operating in the subterahertz regime, roughly 150−660 GHz, and cryogenic MAS probes. In addition, improvements were required in the polarizing agents, because the high concentrations of conventional radicals that are required to produce significant enhancements compromise spectral resolution.

In the last two decades, scientific and technical advances have addressed these problems and brought DNP to the point where it is achieving wide applicability. These advances include the development of high frequency gyrotron microwave sources operating in the subterahertz frequency range. In addition, low temperature MAS probes were developed that permit in situ microwave irradiation of the samples. And, finally, biradical polarizing agents were developed that increased the efficiency of DNP experiments by factors of ∼4 at considerably lower paramagnet concentrations. Collectively, these developments have made it possible to apply DNP on a routine basis to a number of different scientific endeavors, most prominently in the biological and material sciences. This Account reviews these developments, including the primary mechanisms used to transfer polarization in high frequency DNP, and the current choice of microwave sources and biradical polarizing agents. In addition, we illustrate the utility of the technique with a description of applications to membrane and amyloid proteins that emphasizes the unique structural information that is available in these two cases.

## Introduction

Magic angle spinning (MAS) nuclear magnetic resonance (NMR) has emerged as a powerful, nondestructive method that can be used to characterize the structure and dynamics of systems that are not accessible by either solution NMR or crystallography. In particular, the last three decades have witnessed the development of MAS techniques to probe various anisotropic interactions at the molecular and atomic scale via dipole recoupling techniques.[1] As a consequence, it is possible to measure internuclear distances in

Published on the Web 04/18/2013 www.pubs.acs.org/accounts
10.1021/ar300348n 

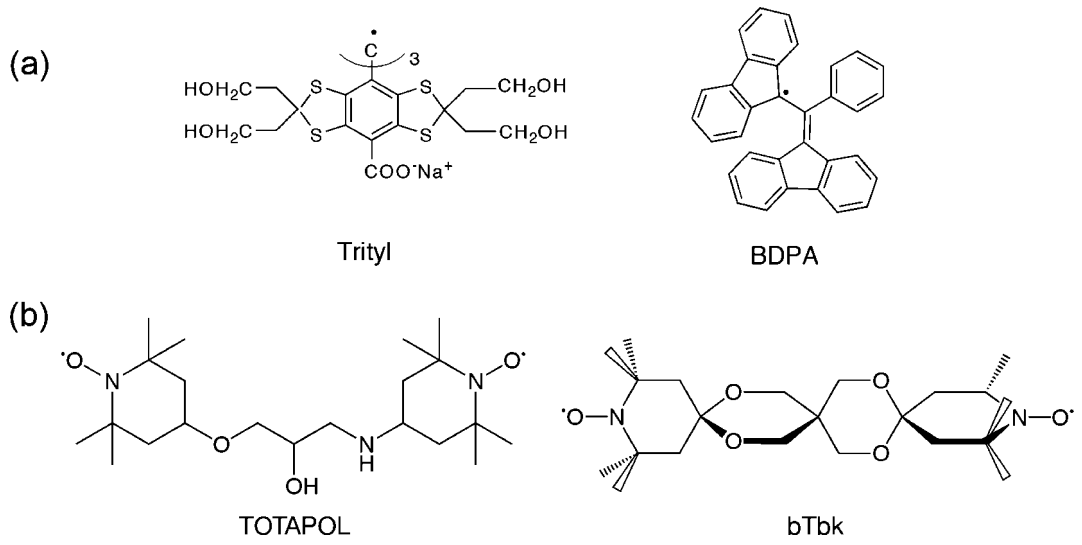


**FIGURE 1.** Polarizing agents commonly used for high field DNP experiments: (a) narrow line radicals trityl and BDPA used for the SE; (b) TEMPO based biradicals TOTAPOL and bis-TEMPO-bis-ketal (bTbk) used for the CE.

amorphous and powder samples as well as in crystals. In principle, these measurements provide copious high resolution information about the structure and dynamics of a variety of biological systems such as peptides,[2] membrane proteins,[3−5] nanocrystals,[6] amyloids,[7−10] and materials science (*vide infra*). Given this versatility, the recent rapid expansion of MAS NMR is expected to continue.

Despite the outstanding progress in this field, there remains an acute sensitivity problem since MAS NMR usually involves direct detection of $^{13}C$, $^{15}N$, or another low-$\gamma$ species. Cross-polarization (CP) techniques and operation at higher magnetic fields have helped to address this issue. However, significantly higher sensitivity would help to bring MAS NMR into a regime where it is truly widely applicable. The subject of this Account is recent $10^2-10^3$ fold improvements in MAS NMR sensitivity based on high frequency dynamic nuclear polarization (DNP). As we will see, high frequency DNP is significantly changing the landscape of what is possible with MAS NMR. This Account illustrates this point with a discussion of polarization transfer mechanisms, polarizing agents, instrumentation, and recent applications of MAS DNP to complex heterogeneous systems.

## DNP Mechanisms

DNP enhances NMR signals by transferring the large polarization of electrons to nearby nuclei via microwave ($\mu$w) irradiation of electron−nuclear transitions.[11] Contemporary MAS DNP experiments on *insulating* solids are usually based on either the solid effect (SE), coupling an electron−nuclear spin pair, or the cross effect (CE), utilizing a pair of electrons in the form of a biradical and a nuclear spin. A third mechanism, thermal mixing (TM), involves multiple electrons and a homogeneously broadened EPR spectrum. However, at the high fields and low temperatures (80−110 K) currently used in MAS experiments, TM has thus far not provided an important polarization pathway. In all of these mechanisms, it is necessary to add a stable paramagnetic polarizing agent to the sample and the most commonly used radicals are shown in Figure 1. Trityl and BDPA (or water-soluble BDPA[12]) support the SE, whereas the TEMPO based biradicals TOTAPOL[13] and bTbk[14] are used for the CE. The detailed polarization transfer schemes discussed below are closely linked to the shapes of the high field EPR spectra of these molecules.

## The Solid Effect

The SE can be understood using a two-spin model involving one electron and one nucleus, interacting via an electron−nuclear dipole coupling, and irradiation at nominally forbidden electron transitions at $\omega_{\mu w} = \omega_{0S} \pm \omega_{0I}$ illustrated in Figure 2. The Hamiltonian applicable to the two spin system is

$$\hat{H} = \omega_{0S}\hat{S}_z - \omega_{0I}\hat{I}_z + C\hat{S}_z\hat{I}_+ + C^*\hat{S}_z\hat{I}_-$$

where $\omega_{0S}$ and $\omega_{0I}$ are the electron and nuclear Larmor frequencies, respectively, $C=(-3/2)(\gamma_S\gamma_I/r_{IS}^3)\sin\theta\cos\theta\, e^{-i\phi}$ is the usual term in the electron−nuclear dipole Hamiltonian[15] and $S$ and $I$ are spin operators for electrons and nuclei, respectively. First order perturbation theory yields the mixed eigenstates shown in Figure 2, where the

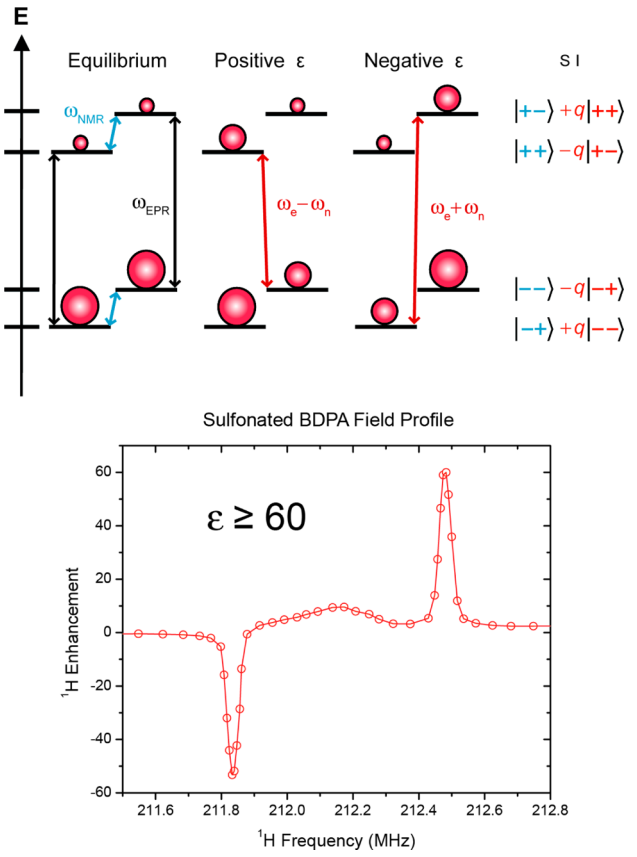


**FIGURE 2.** (top) Energy level diagram illustrating DNP via the solid effect (SE). At thermal equilibrium (left), populations are governed by the Boltzmann distribution. Mixing of states in the electron spin subspaces (right) leads to partially allowed double quantum (DQ) and zero quantum (ZQ) transitions, and positive and negative enhancements, $\varepsilon$, respectively. The mixing of states is proportional to a constant $q$, which is inversely proportional to $B_0$. Therefore, the enhancement in the solid effect DNP scales as $B_0^{-2}$. (bottom) Plot of the enhancement from SA-BDPA[12] as a function of magnetic field ($^1$H frequency) showing the positive and negative enhancements. $\omega_{NMR}$ and $\omega_{EPR}$ are the NMR and EPR frequencies, and $\omega_e \pm \omega_n$ are the sum and difference of the EPR and NMR frequencies, respectively.

mixing coefficient $q = C/2\omega_{0I} \ll 1$. The other terms in the electron–nuclear dipolar Hamiltonian (*A*, *B*, *E*, and *F* in Van Vleck notation) also mix states, but the contributions are relatively small. Irradiation of the partially allowed transitions by $\mu$w's gives rise to either positive (double quantum) or negative (zero quantum) enhancement of the nuclear polarization as illustrated at the bottom of Figure 2.

The SE is the dominant DNP mechanism in systems where the polarizing agent exhibits a homogeneous EPR line width ($\delta$) and an inhomogeneous spectral breadth ($\Delta$) smaller than the nuclear Larmor frequency ($\delta, \Delta < \omega_{0I}$). This condition is satisfied by radicals with high molecular symmetry such as BDPA,[16] SA-BDPA,[12] and trityl OX063,[17] where the g tensors are nearly isotropic and the hyperfine interaction is small. However, as the SE relies on the mixing of nuclear states by electron–nuclear coupling, the enhancement scales as $\omega_{0I}^{-2}$. Therefore, the SE becomes less efficient at high magnetic fields (>3 T). Nevertheless, recent research suggests that SE can be very efficient at high field provided that high microwave power, and a large $\omega_{1S} = \gamma_e B_{1S}$ is available. Enhancements as high as ~144 have been achieved at 5 T. Finally, the SE can also be the dominant mechanism when transition metals complexes, for example, with $Gd^{3+}$, are used as polarizing agents. Since the broadening of the EPR line in these systems is mainly induced by the zero field splitting, the EPR line narrows at higher magnetic fields and metal-based polarizing agents may show improved performances at higher fields.[18]

## The Cross Effect

When $\Delta > \omega_{0I} > \delta$, DNP is governed by the CE and scales with $\omega_{0I}^{-1}$, leading to larger enhancements at higher magnetic fields. At high fields, where the EPR spectrum is dominated by g-anisotropy and inhomogeneously broadened, a three spin quantum mechanical treatment is possible.[19–21] The Hamiltonian for the nuclear spin and two electrons is

$$\hat{H} = \omega_{0S_1}\hat{S}_{1z} + \omega_{0S_2}\hat{S}_{2z} - \omega_{0I}\hat{I}_z + (A_1\hat{S}_{1z} + A_2\hat{S}_{2z})\hat{I}_z + (B_1\hat{S}_{1z} + B_2\hat{S}_{2z})\hat{I}_x + d(3\hat{S}_{1z}\hat{S}_{2z} - \vec{S}_1\cdot\vec{S}_2) - 2J\vec{S}_1\cdot\vec{S}_2$$

where the first three terms represent electron and nuclear Zeeman interactions, the fourth and fifth describe the electron–nuclear coupling (with A and B denoting the secular and pseudosecular hyperfine couplings[22]), the sixth represents the electron–electron dipolar coupling, and the last describes exchange coupling. This leads to the energy level diagram for the CE is shown in Figure 3, and electron–electron–nuclear polarization transfer is maximized when the central energy levels are degenerate. This occurs when the matching condition $|\omega_{0S_1} - \omega_{0S_2}| = \omega_{0I}$ is fulfilled, where $\omega_{0S_1}$ and $\omega_{0S_2}$ are the Larmor frequencies of dipolar coupled electrons $S_1$ and $S_2$. The degeneracy leads to saturation of the four connected levels and enhanced nuclear polarization. A field profile obtained from bTbk is shown at the bottom of Figure 3, and roughly represents the negative first derivative of the EPR spectrum. Also shown are the positions in the EPR powder pattern that are irradiated for optimal positive and negative enhancements.

Initially, high-field CE DNP experiments were performed with monoradical species, such as TEMPO.[23,24] In this

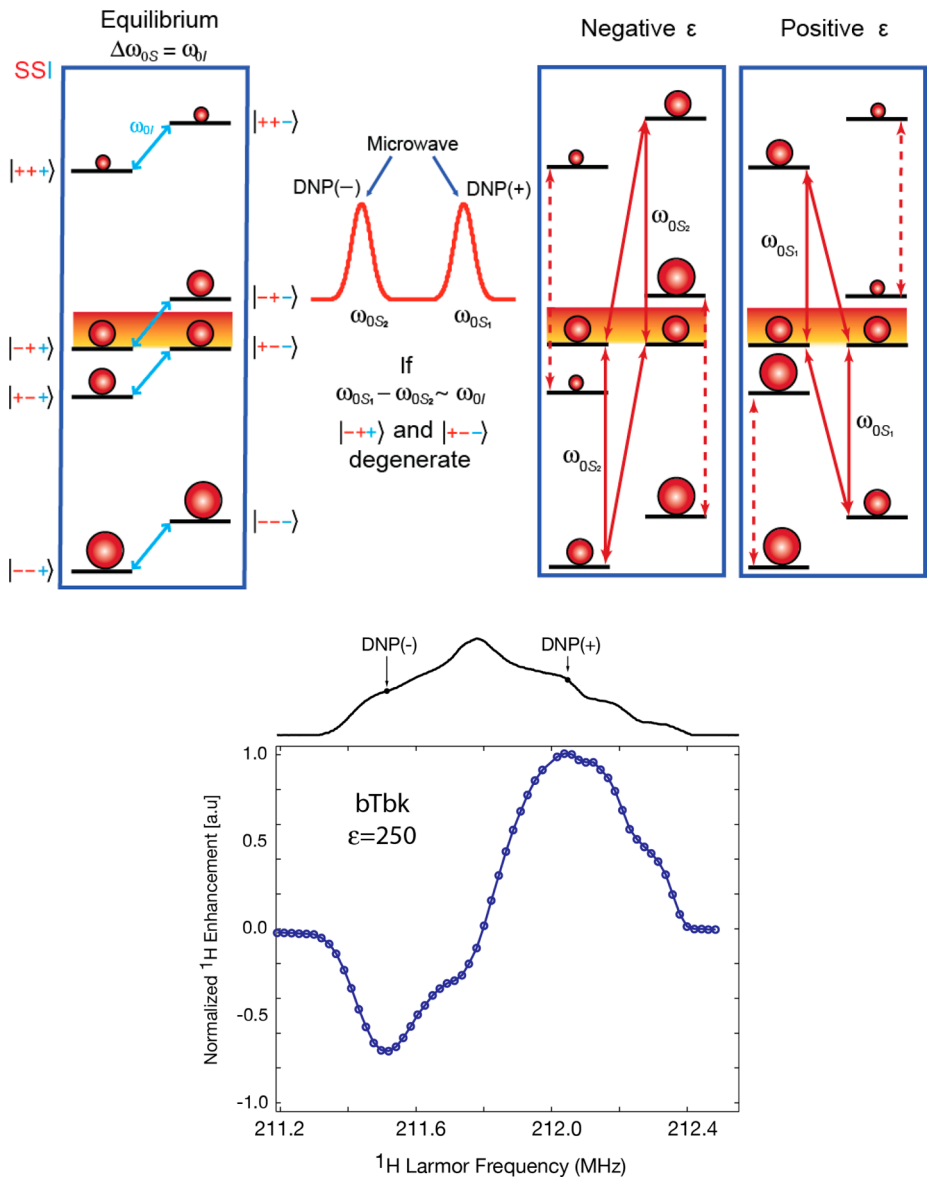


**FIGURE 3.** (top) Energy diagram illustrating DNP via the CE. At equilibrium (left), under the matching condition, there is degeneracy and 1:1 population of the two shaded levels. The EPR spectrum of an ideal biradical for CE (middle) has two narrow lines separated by the nuclear Larmor frequency. Saturation of transitions near the first (second) EPR line gives rise to a positive (negative) DNP enhancement (right). (bottom) Field profile for bTbk with an enhancement $\varepsilon = 250$.[14]

situation, the frequency matching condition is fulfilled only for the fraction of the radicals that adopt the correct relative orientation of their g-tensors. In order to improve CE DNP, we introduced biradicals such as bis-TEMPO-*n*-ethylene glycol (BTnE)[19] and TOTAPOL,[13] consisting of two tethered TEMPO moieties to obtain relatively short (~12 Å) electron−electron distances independent of concentration. With these polarizing agents, which have an e−e dipole coupling of 20−30 MHz, the enhancements were ~4-fold higher at an ~4-fold lower electron concentration. Figure 4 shows recent results obtained using TOTAPOL from two standard samples, urea and proline. The observed $\varepsilon = 181$ and $\varepsilon = 134$ are ~2-fold higher than we initially reported for TOTAPOL at this field[25] due to improvements in instrumentation, primarily gyrotron output power and lower temperatures (*vide infra*).

## Optimizing DNP Signal Enhancements

DNP enhancements are governed by a number of factors, including microwave power, concentration and design of the polarizing agent, temperature, solvent, and the relaxation times of the solvent and solute. We now review recent results aimed at optimizing the efficiency of DNP experiments with a focus on the influence of these parameters on the enhancements.

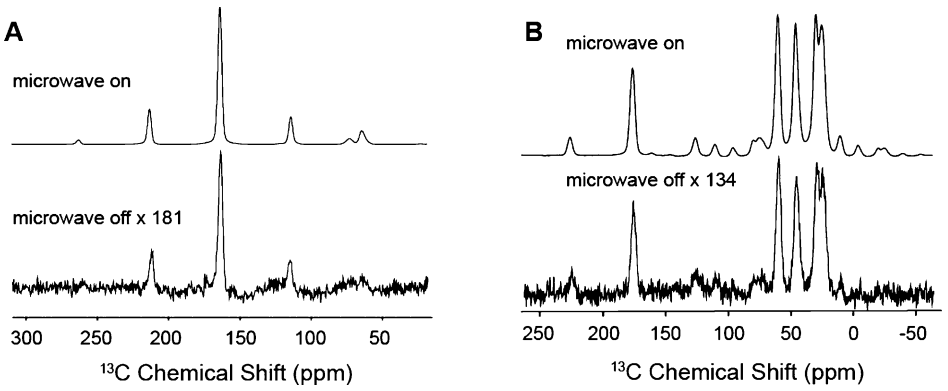


**FIGURE 4.** $^{13}$C CP MAS NMR spectra of (A) 1 M U-[$^{13}$C−$^{15}$N] urea and (B) 0.5 M U-[$^{13}$C−$^{15}$N] proline at 80 K with and without microwave irradiation. The DNP enhancements are $\varepsilon = 181$ and $\varepsilon = 134$, respectively. Both samples contained 10 mM TOTAPOL in a 60/30/10 volume ratio of $d_8$-glycerol/$D_2O$/$H_2O$. Experimental parameters are as follows: 4 scans, recycle delay 4 s, microwave power ~12.5 W, $\gamma B_1(^1H) = 83$ kHz for excitation pulse and decoupling, 50 kHz for CP. The CP was optimized by scanning the $\gamma B_1(^{13}C)$ up to 71 kHz.

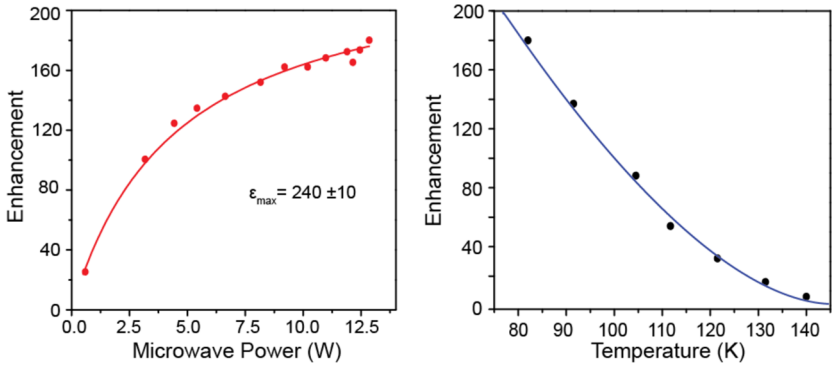


**FIGURE 5.** $^{13}$C CP DNP enhancements of 1 M U-[$^{13}$C, $^{15}$N] urea with 10 mM TOTAPOL plotted as a function of $\mu$w power at 80 K (left) and as a function of temperature at 12.5 W $\mu$w (right). $\omega_r/2\pi = 7$ kHz.

**Microwave Power.** Gyrotrons[16,26,27] are capable of producing tens of watts of $\mu$w power with excellent frequency stability and low phase noise, making them the current microwave source of choice for DNP experiments. In particular, the low $Q$ of the microwave circuit in the MAS NMR probe necessitates copious power to generate a sufficient $B_1$ to excite DNP transitions. Furthermore, since the gyrotron is a fast wave device, it can operate at high powers for extended periods of time, as is required for multidimensional NMR experiments that involve signal averaging. Figure 5 (left) shows the enhancement as a function of $\mu$w power at 80 K obtained with a frequency tunable 250 GHz gyrotron.[28] The enhancement increases with power, does not saturate at our maximum available power of 12.5 W, and extrapolates to a limiting value $\varepsilon_{max} \sim 240$. Similar dependences of $\varepsilon$ on $\mu$w power have been published elsewhere.[29,30] An alternative microwave source, that we explored sometime ago and currently in use in some laboratories,[31] is a low power (~10−100 mW) Gunn diode. However, the enhancements are lower: on one sample, $\varepsilon \sim 25$ with 10 mW from the Gunn diode versus $\varepsilon = 185$ with 1 W from the gyrotron.[32] Thus, the data in Figure 5 suggest that with current technology the gyrotron is the microwave source of choice for DNP experiments, especially at microwave/ $^1$H NMR frequencies ≥ 263 GHz/400 MHz for e/$^1$H. Currently gyrotron-based DNP spectrometers are operating at microwave/$^1$H NMR frequencies up to 460 GHz/700 MHz[29] and are expected to go still higher. Nevertheless, microwave technology does improve with time, and it is possible that alternatives to the gyrotron and Gunn diode will be available in the future.

**Temperature and Polarizing Agents.** Both the sample temperature and the nature of the polarizing agent profoundly influence the DNP enhancements. Lower temperatures improve both the SE and CE enhancements, most likely due to the longer proton relaxation times. Figure 5 (right) plots recent data showing the temperature dependence of the $^1$H DNP signal enhancement in the range 80−140 K at 250 GHz/380 MHz with the TOTAPOL/urea sample described above. Note that the DNP enhancement increases as the temperature approaches 80 K, by a factor of 3.6 in the range 110−80 K.

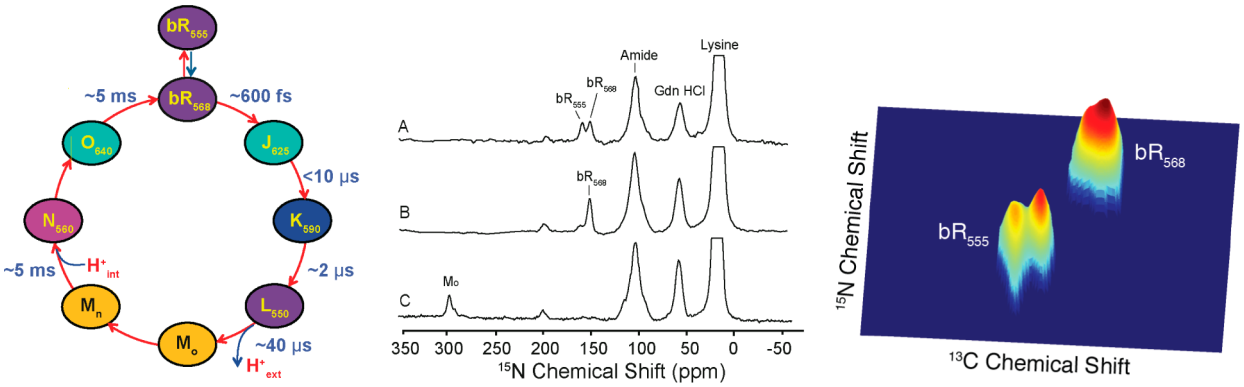


**FIGURE 6.** (left) Ion-motive photocycle of bR. The subscript for each intermediate represents the wavelength (in nm) of maximum visible absorption. (middle) $^{15}$N CP DNP spectra [$\zeta$-$^{15}$N-Lys] bR prepared with 15 mM TOTAPOL in 60/30/10 ratio of $d_8$-glycerol/$D_2O$/$H_2O$ in 0.3 M guanidinium hydrochloride at pH 10. (A) The dark adapted (DA) state comprises a thermal equilibrium mixture of $bR_{555}$ and $bR_{568}$. (B) Light Adapted (LA) ($bR_{568}$) accumulated by 532 nm irradiation of the rotating sample for 4 h at 273 K. (C) Mo intermediate created by 532 nm irradiation of rotating LA at 230 K. The spectra of all three intermediates were obtained in roughly 2 h with a spinning frequency of 7 kHz. (right) 2D spectrum obtained from DA bR illustrating the splittings observed at low temperature due to inequivalent sites.

It is well-known that high concentrations of paramagnets dramatically broaden NMR linewidths and attenuate integrated NMR signal intensities. It is for this reason that we developed biradical polarizing agents with a ~20−30 MHz intramolecular e−e dipole coupling which yield ~4-fold larger enhancements at ~4-fold lower electron concentration than monoradicals such as TEMPO.[19] Our experiments performed on urea, proline, bacteriorhodopsin (bR), and PI3-SH3 fibrils[33,34] suggest that optimal radical concentration of TOTAPOL is 10−20 mM.

Finally, we note that biradicals such as bTbk[14] (Figure 1) and bTbk-py[35] have the TEMPO moieties locked at ~90° with respect to one another, and therefore yield a relative orientation of the two g-tensors that better satisfies the CE matching condition. These polarizing agents have produced enhancements as large as 250 (Figure 3).[14]

It was previously reported that $^2$H labeled solvents improve $^1$H DNP enhancements, and that even with 90−95% $^2$H labeling we can still efficiently CP to low gamma nuclei in the target molecule.[19,36] Thus, while $^1$H dilution attenuates relaxation processes, even dilute protons mediate $^1$H−$^1$H spin diffusion, with the overall result of a higher enhancement. For example, Akbey et al.[37] reported that perdeuteration of the $\alpha$-spectrin-SH3 domain led to three to five times higher DNP enhancement ($\varepsilon \sim 148$) than obtained with protonated SH3. In a more recent example we prepared 98% perdeuterated U-[$^2$H,$^{13}$C,$^{15}$N] bR and with 15 mM TOTAPOL and observed $\varepsilon = 72$, whereas for U-[$^1$H, $^{13}$C,$^{15}$N]-bR we obtained $\varepsilon \sim 35-43$.[33,38] Thus, perdeuterated proteins will likely be important for biological applications of DNP.

**Applications of DNP MAS NMR.** To date one of the most interesting examples of the application of DNP is to the light-driven ion pump bR, which is a 26.6 kDa trans-membrane protein containing a retinal chromophore. bR has been studied intensively since its discovery in the 1970s, but the mechanism by which it enforces vectorial action is still not understood and MAS NMR studies can potentially elucidate the relevant structural details of the intermediates in its photocycle (Figure 6 (left)). However, many of the intermediates can only be cryo-trapped at low (~5%) concentrations, so that high signal-to-noise, and therefore DNP, is required to observe their MAS NMR spectra.[33,38]

The retinal cofactor is covalently bonded to Lys216 via a protonated Schiff base linkage, and the sensitivity of the unique $^{15}$N chemical shift of the Schiff base to its local environment provides an excellent marker and probe of each photocycle intermediate. In the dark-adapted (DA) state, bR exhibits two conformations: $bR_{555}$ and $bR_{568}$ in a ratio of 60:40 (Figure 6 (middle, A)). After irradiation at 532 nm, DA is converted to light adapted (LA) state in which only $bR_{568}$ remains (Figure 6 (middle, B)). Upon the absorption of a photon, the retinal isomerizes and cycles the protein through several intermediates that can be cryo-trapped for observation in situ. Figure 6 (middle, C) shows the 1D spectrum of $M_o$. With low temperature DNP it is possible to perform 2D spectroscopy and a $^{13}$C−$^{15}$N spectrum of DA bR is shown in Figure 6 (right) showing that at 90 K there are actually four forms of bR present, two each of the $bR_{555}$ and $bR_{568}$.

We have also published the first DNP MAS NMR spectra of the K and L intermediates.[33,38] While the K state showed just one Schiff base signal, it relaxed to several L states, of which all but one are dead ends (relaxing back to bR). The data for the functional L state (the one that relaxes to M) suggest that its Schiff base has a strong counterion. One of

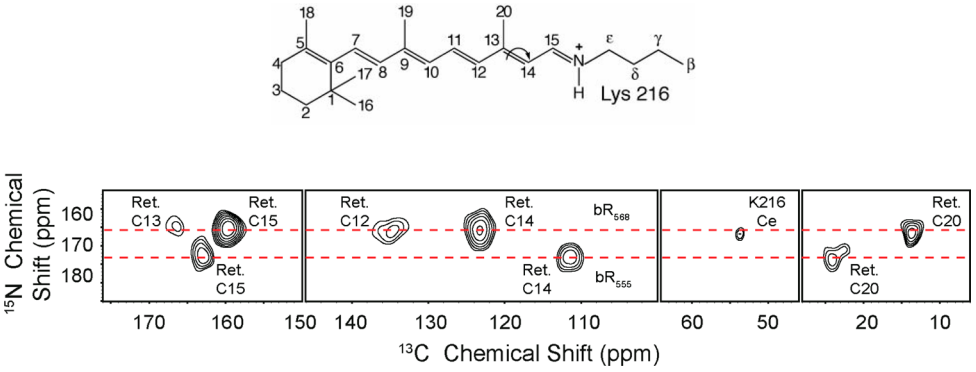


**FIGURE 7.** $^{15}$N−$^{13}$C spectrum obtained from dark adapted U-[$^{13}$C,$^{15}$N]-bR after selective excitation of the $^{15}$N Schiff base, CP to the $^{13}$C-15 of the retinal and $^{13}$C$\varepsilon$ of Lys216, followed by RFDR mixing. The spectrum shows cross-peaks between the Schiff base $^{15}$N and $^{13}$C-12,13,14,15,20 on the retinal chromophore and $^{13}$C$\varepsilon$ Lys216.[27,33,39] The arrow indicates the *trans*−*cis* isomerization of the C13=C14 bond that occurs during the photocycle.

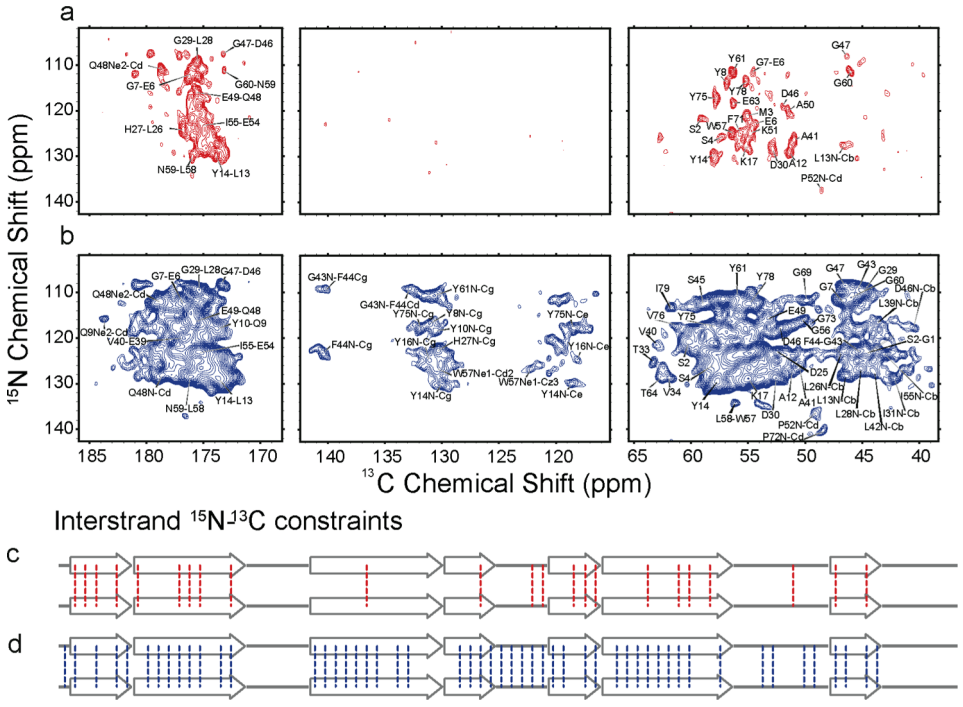


**FIGURE 8.** Comparison between room temperature and DNP enhanced, low temperature correlation spectra of PI3-SH3. The spectra were obtained with ZF-TEDOR recoupling ($\tau_{mix}$ = 16 ms) from sample prepared from partially labeled fibrils [$^{15}$N, $^{12}$C] PI3-SH3 /[ $^{14}$N,$^{13}$C] PI3-SH3 (50:50 molar ratio). (a) $^{15}$N−$^{13}$C intermolecular correlations in PI3-SH3 fibrils at 300 K obtained at 750 MHz in 16 days of acquisition time. (b). Same sample and identical spectral regions were recorded at 100 K and 400 MHz with DNP enhancement in 32 h. (c). Illustration of the 23 interstrand contacts established from $^{13}$C -$^{15}$N peaks in the 750 MHz spectra acquired at 300 K in a. (d) the 52 interstrand contacts established from the 400 MHz DNP enhanced spectra recorded at 100 K shown in (d).[34]

the possible explanations would support the hypothesis that bR is an inward $OH^-$ pump, rather than an outward $H^+$ pump.

With the sensitivity available from DNP, it is also possible to record 2D correlation spectra for the individual resonances in the DA state which has an effective molecular weight of ~85 kDa. Figure 7 shows cross-peaks between the Schiff base $^{15}$N and $^{13}$C-12,13,14,15,20 of the retinal and $^{13}$C-$\varepsilon$ of Lys216 in the dark adapted state of bR. The experiment has been conducted by using a Gaussian pulse to select the signals arising from the $^{15}$N of Lys216 in both bR$_{568}$ and bR$_{555}$ followed by a $^{15}$N−$^{13}$C and then $^{13}$C−$^{13}$C diffusion via RFDR mixing. Again the spectrum of bR would not be accessible *sans* DNP.

**Amyloid Fibrils.** MAS NMR is also essential for studies of the structure of amyloid fibrils. Intermolecular $^{13}$C−$^{13}$C or $^{15}$N−$^{13}$C distances derived from MAS DNP experiments provide otherwise unavailable structural constraints. The most straightforward approach is to measure long-range $^{13}$C−$^{15}$N distances with a ZF-TEDOR experiment.[40] However, for

distances ≥ 5 Å, the efficiency is low (<5%), which vastly extends the acquisition time and severely limits the number of constraints that can be observed. The application of DNP to overcome this situation has been demonstrated on mixed samples of [$^{15}$N, $^{12}$C] PI3-SH3/[ $^{14}$N,$^{13}$C] PI3-SH3 (50:50 molar ratio). Figure 8 compares the $^{15}$N−$^{13}$C intermolecular correlation spectra obtained with ZF-TEDOR recoupling ($\tau_{mix}$ = 16 ms) at 750 MHz without DNP and at 400 MHz with DNP, collected in 16 days and 32 h, respectively. The number of intermolecular $^{15}$N−$^{13}$C constraints detected was more than doubled due to the DNP with $\varepsilon \sim 30$ on $^{13}$C. The additional constraints obtained from DNP permitted us to establish that the PI3-SH3 protein strands are aligned in a parallel and in-register $\beta$-sheet arrangement.[34]

In addition, it is clear that the approaches described here are widely applicable to other areas of science, in particular materials problems: polymers, zeolites, surfaces, semiconductors, and so forth. These experiments will likely include spectroscopy of quadrupolar species such as $^{17}$O[41] and $^{27}$Al[42] as well as $I = 1/2$ species. We refer the interested reader to other articles in this issue for a complete discussion of these very interesting applications.

Finally we note that, while most of the results described here were obtained at 250 GHz/380 MHz or 263 GHz/400 MHz, DNP experiments have recently been performed at 460 GHz/700 MHz[29] and at 395 GHz/600 MHz and 527 GHz/800 MHz [http://www.bruker.com/products/mr/nmr/dnp-nmr/overview.html]. Thus, DNP is rapidly moving to higher frequency where the chemical shift resolution will improve and additional systems will become accessible.

## Conclusions

There are currently two important mechanisms that mediate high field DNP processes, namely, the SE and the CE. In addition, there are a number of important experimental factors that influence the magnitudes of the enhancements, including microwave power, temperature, and the nature of the polarizing agent. With currently available technology (gyrotron microwave sources, MAS at 80 K, biradical polarizing agents, and partially deuterated proteins), it is possible to obtain enhancements of ≥100 on many samples. This enhancement, together with the improved Boltzmann factor of 300 K/80 K = 3.75 due to the lower temperature, yields sensitivity gains of ≥375 and time savings of >$10^5$. Historically, increases in sensitivity of NMR experiments by factors of $10^2$−$10^3$ have dramatically changed the landscape of what is possible with NMR, and we are beginning to witness the next step in this movement due to high frequency DNP. We have illustrated this point with applications of MAS DNP experiments to membrane proteins and fibrils which are typical of the biological materials that will be studied in the future. These results clearly illustrate that many experiments that are not possible *sans* DNP, become feasible *avec* DNP. Thus, it is clear that the increased availability of commercial instruments to perform DNP experiments will open many new avenues of scientific and technical endeavor.

*We thank Drs. Alexander Barnes, Bjorn Corzilius, Yongchao Su, Marvin J. Bayro Christopher Turner, and David J. Ruben for their insightful discussions and Jeffrey Bryrant, and Ajay Thakkar, for their extensive technical assistance. This work was supported by National Institute of Health Grants EB002804, EB001960, EB003151, EB001035, GM095843, and EB002026.*

**Note Added after ASAP Publication.** This paper published on the Web on April 18, 2013. Changes were made in the text and Figure 5 was replaced. The revised version was reposted on April 25, 2013.

BIOGRAPHICAL INFORMATION

**Qing Zhe Ni** received a B.S. degree in chemistry, with minors in physics and mathematics, summa cum laude from Florida State University in 2010. She is currently pursuing the Ph.D. degree in the Department of Chemistry at MIT.

**Eugenio Daviso** received his Laurea degree in Industrial Chemistry from the Università degli Studi di Torino in 2001, and his Ph.D. in Chemistry with Prof. Huub de Groot and Dr. Joerg Matysik in The Netherlands in 2008. He is currently a postdoc at the Francis Bitter Magnet Laboratory and Department of Chemistry, MIT.

**Thach V. Can** studied physics at Vietnam National University, Hanoi, and then received his M.S. from the Florida State University. Currently he is a Ph.D. student in the Department of Chemistry at MIT.

**Evgeny Markhasin** obtained his M.S. degree from the University of Nizhniy Novogorod in Russia and is currently a Ph.D. student in the Chemistry Department at MIT.

**Sudheer K. Jawla** received his M.Sc. degree in physics from the IIT-Delhi, New Delhi, India, in 2004 and Ph.D. degree in physics from the EPFL, Lausanne, Switzerland in 2010. He is currently a postdoc at Plasma Science and Fusion Center, MIT.

**Timothy M. Swager** received his B.S. from Montana State University and Ph.D. from CalTech. He is currently Professor of Chemistry at MIT, and one of his many interests is the synthesis of new polarizing agents for DNP.

**Richard J. Temkin** received his B.A. degree in physics from Harvard College, and his M.A. and Ph.D. degrees in physics from MIT. Since 1974, he has been with MIT, first at the Francis Bitter National Magnet Laboratory and later at the Plasma Science and Fusion Center (PSFC) and the Department of Physics.

**Judy Herzfeld** received her B.A. degree in Chemistry from the Barnard College in 1967, her Ph.D. in chemical physics from MIT in

1972, and an M.P.P. from the Kennedy School of Government at Harvard University in 1973. She has served on the faculties of Amherst College, Harvard Medical School, and, since 1985, the Department of Chemistry at Brandeis University.

**Robert G. Griffin** received his B.S. degree in 1964 from the University of Arkansas, and his Ph.D. from Washington University, St. Louis, MO, in 1969. He has been at the Francis Bitter Magnet Laboratory since 1972 and a faculty member in the Department of Chemistry at MIT since 1989.

## FOOTNOTES

*To whom correspondence should be addressed. E-mail: rgg@mit.edu.
The authors declare no competing financial interest.
Q.Z.N. and E.D. contributed equally. The manuscript was written through contributions of all authors. All authors have given approval to the final version of the manuscript.

## REFERENCES


1 Griffin, R. G. Dipolar recoupling in MAS spectra of biological solids. *Nat. Struct. Biol.* **1998**, *5*, 508–512.

2 Rienstra, C. M.; Hohwy, M.; Mueller, L. J.; Jaroniec, C. P.; Reif, B.; Griffin, R. G. Determination of multiple torsion-angle constraints in U-13C,15N-labeled peptides: 3D 1H-15N-13C-1H dipolar chemical shift spectroscopy in rotating solids. *J. Am. Chem. Soc.* **2002**, *124*, 11908–11922.

3 Thompson, L. K.; McDermott, A. E.; Raap, J.; van der Wielen, C. M.; Lugtenburg, J.; Herzfeld, J.; Griffin, R. G. Rotational Resonance NMR Study of the Active Site Structure in Bacteriorhodopsin: COnformation of the Schiff Base Linkage. *Biochemistry* **1992**, *31*, 7931.

4 Griffiths, J. M.; Lakshmi, K. V.; Bennett, A. E.; Raap, J.; Vanderwielen, C. M.; Lugtenburg, J.; Herzfeld, J.; Griffin, R. G. Dipolar Correlation NMR-Spectroscopy of a Membrane-Protein. *J. Am. Chem. Soc.* **1994**, *116*, 10178–10181.

5 Cady, S. D.; Schmidt-Rohr, K.; Wang, J.; Soto, C.; DeGrado, W.; Hong, M. Structure of the amantadine binding site of influenza M2 proton channels in lipid bilayers. *Nature* **2010**, *463*, 689–692.

6 Castellani, F.; van Rossum, B.; Diehl, A.; Schubert, M.; Rehbein, K.; Oschkinat, H. Structure of a protein determined by solid-state magic-angle-spinning NMR spectroscopy. *Nature* **2002**, *420*, 98–102.

7 Jaroniec, C. P.; MacPhee, C. E.; Bajaj, V. S.; McMahon, M. T.; Dobson, C. M.; Griffin, R. G. High Resolution Molecular Structure of a Peptide in an Amyloid Fibril Determined by MAS NMR Spectroscopy. *Proc. Natl. Acad. Sci. U.S.A.* **2004**, *101*, 711–716.

8 Tycko, R. Molecular structure of amyloid fibrils: insights from solid-state NMR. *Q. Rev. Biophys.* **2006**, *39*, 1–55.

9 Wasmer, C.; Lange, A.; Van Melckebeke, H.; Siemer, A. B.; Riek, R.; Meier, B. H. Amyloid fibrils of the HET-s(218−289) prion form a beta solenoid with a triangular hydrophobic core. *Science* **2008**, *319*, 1523–1526.

10 Bayro, M. J.; Maly, T.; Birkett, N.; MacPhee, C.; Dobson, C. M.; Griffin, R. G. High-resolution MAS NMR analysis of PI3-SH3 amyloid fibrils: Backbone conformation and implications for protofilament assembly and structure. *Biochemistry* **2010**, *49*, 7474–7488.

11 Maly, T.; Debelouchina, G. T.; Bajaj, V. S.; Hu, K.-N.; Joo, C.-G.; Mak-Jurkauskas, M. L.; Sirigiri, J. R.; Wel, P. C. A. v. d.; Herzfeld, J.; Temkin, R. J.; Griffin, R. G. Dynamic Nuclear Polarization at High Magnetic Fields. *J. Chem. Phys.* **2008**, *128*, 052211.

12 Haze, O.; Corzilius, B.; Smith, A. A.; Griffin, R. G.; Swager, T. M. Water-Soluble Narrow-Line Radicals for Dynamic Nuclear Polarization. *J. Am. Chem. Soc.* **2012**, *134*, 14287–14290.

13 Song, C.; Hu, K.-N.; Joo, C.-G.; Swager, T. M.; Griffin, R. G. TOTAPOL − A Biradical Polarizing Agent for Dynamic Nuclear Polarization Experiments in Aqueous Media. *J. Am. Chem. Soc.* **2006**, *128*, 11385–90.

14 Matsuki, Y.; Maly, T.; Ouari, O.; Lyubenova, S.; Herzfeld, J.; Prisner, T.; Tordo, P.; Griffin, R. G. Dynamic Nuclear Polarization using a Rigid Biradical. *Angew. Chem.* **2009**, *48*, 4996–5000.

15 Goldman, M. *Spin Temperature and Nuclear Magnetic Resonance in Solids*; Oxford University Press: London, 1970.

16 Becerra, L. R.; Gerfen, G. J.; Temkin, R. J.; Singel, D. J.; Griffin, R. G. Dynamic Nuclear Polarization with a Cyclotron Resonance Maser at 5 T. *Phys. Rev. Lett.* **1993**, *71*, 3561–3564.

17 Ardenkjaer-Larsen, J. H.; Laursen, I.; Leunbach, I.; Ehnholm, G.; Wistrand, L. G.; Petersson, J. S.; Golman, K. EPR and DNP properties of certain novel single electron contrast agents intended for oximetric imaging. *J. Magn. Reson.* **1998**, *133*, 1–12.

18 Corzilius, B.; Smith, A. A.; Barnes, A. B.; Luchinat, C.; Bertini, I.; Griffin, R. G. High Field Dynamic Nuclear Polarization with High-Spin Transition Metal Ions. *J. Am. Chem. Soc* **2011**, *133*, 5648–5651.

19 Ardenkjaer-Larsen, J. H.; Laursen, I.; Leunbach, I.; Ehnholm, G.; Wistrand, L. G.; Petersson, J. S.; Golman, K. EPR and DNP properties of certain novel single electron contrast agents intended for oximetric imaging. *J. Magn. Reson.* **1998**, *133*, 1–12.

20 Hu, K.-N.; Song, C.; Yu, H.-h.; Swager, T. M.; Griffin, R. G. High-Frequency Dynamic Nuclear Polarization Using Biradicals: A Multifrequency EPR Lineshape Analysis. *J. Chem. Phys.* **2008**, *128*, 052321.

21 Hu, K.-N.; Debelouchina, G. T.; Smith, A. A.; Griffin, R. G. Quantum mechanical theory of dynamic nuclear polarization in solid dielectrics. *J. Chem. Phys.* **2011**, *134*, 125105.

22 Schweiger, A.; Jeschke, G. *Principles of pulsed electron paramagnetic resonance*; Oxford University Press: Oxford, UK, 2001.

23 Bajaj, V. S.; Farrar, C. T.; Hornstein, M. K.; Mastovsky, I.; Vieregg, J.; Bryant, J.; Elena, B.; Kreischer, K. E.; Temkin, R. J.; Griffin, R. G. Dynamic nuclear polarization at 9T using a novel 250 GHz gyrotron microwave source. *J. Magn. Reson.* **2003**, *160*, 85–90.

24 Rosay, M.; Lansing, J. C.; Haddad, K. C.; Bachovchin, W. W.; Herzfeld, J.; Temkin, R. J.; Griffin, R. G. High Frequency Dynamic Nuclear Polarization in MAS Spectra of Membrane and Soluble Proteins. *J. Am. Chem. Soc.* **2003**, *125*, 13626–27.

25 Barnes, A. B.; Corzilius, B.; Mak-Jurkauskas, M. L.; Andreas, L. B.; Bajaj, V. S.; Matsuki, Y.; Belenky, M. L.; Lugtenburg, J.; Sirigiri, J. R.; Temkin, R. J.; Herzfeld, J.; Griffin, R. G. Resolution and polarization distribution in cryogenic DNP/MAS experiments. *Phys. Chem. Chem. Phys.* **2010**, 12.

26 Becerra, L. R.; Gerfen, G. J.; Bellew, B. F.; Bryant, J. A.; Hall, D. A.; Inati, S. J.; Weber, R. T.; Un, S.; Prisner, T. F.; McDermott, A. E.; Fishbein, K. W.; Kreischer, K. E.; Temkin, R. J.; Singel, D. J.; Griffin, R. G. A Spectrometer for Dynamic Nuclear-Polarization and Electron-Paramagnetic-Resonance at High-Frequencies. *J. Magn. Reson., Ser. A* **1995**, *117*, 28–40.

27 Bajaj, V. S.; Hornstein, M. K.; Kreischer, K. E.; Sirigiri, J. R.; Woskov, P. P.; Mak-Jurkauskas, M. L.; Herzfeld, J.; Temkin, R. J.; Griffin, R. G. 250 GHz CW gyrotron oscillator for dynamic nuclear polarization in biological solid state NMR. *J. Magn. Reson.* **2007**, *189*, 251–279.

28 Barnes, A. B.; Nanni, E. A.; Griffin, R. G.; Temkin, R. J. A 250 GHz gyrotron with a 3 GHz tuning bandwidth for dynamic nuclear polarization. *J. Magn. Reson.* **2012**, *221*, 147–153.

29 Barnes, A. B.; Markhasin, E.; Daviso, E.; Michaelis, V. K.; Nanni, E. A.; Jawla, S.; Mena, E.; DeRocher, R.; Thakkar, A.; Woskow, P.; J. Herzfeld, R. J. T.; Griffin, R. G. Dynamic Nuclear Polarization at 700 MHz/460 GHz. *J. Magn. Reson.* **2012**, *221*, 1–7.

30 Barnes, A. B.; Mak-Jurkauskas, M. L.; Matsuki, Y.; Bajaj, V. S.; Wel, P. C. A. v. d.; DeRocher, R.; Bryant, J.; Sirigiri, J. R.; Temkin, R. J.; Lugtenburg, J.; Herzfeld, J.; Griffin, R. G. Cryogenic sample exchange NMR probe for magic angle spinning dynamic nuclear polarization. *J. Magn. Reson.* **2009**, *198*, 261–270.

31 Thurber, K. R.; Yau, W.-M.; Tycko, R. Low-temperature dynamic nuclear polarization at 9.4 T with a 30 mW microwave source. *J. Magn. Reson.* **2010**, *204*, 303–313.

32 Gerfen, G. J.; Becerra, L. R.; Hall, D. A.; Griffin, R. G.; Temkin, R. J.; Singel, D. J. High-Frequency (140 GHz) Dynamic Nuclear-Polarization - Polarization Transfer to a Solute in Frozen Aqueous-Solution. *J. Chem. Phys.* **1995**, *102*, 9494–9497.

33 Gerfen, G. J.; Becerra, L. R.; Hall, D. A.; Griffin, R. G.; Temkin, R. J.; Singel, D. J. High-Frequency (140 GHz) Dynamic Nuclear-Polarization - Polarization Transfer to a Solute in Frozen Aqueous-Solution. *J. Chem. Phys.* **1995**, *102*, 9494–9497.

34 Bayro, M. J.; Debelouchina, G. T.; Eddy, M. T.; Birkett, N. R.; MacPhee, C. E.; Rosay, M.; Maas, W. E.; Dobson, C. M.; Griffin, R. G. Intermolecular structure determination of amyloid fibrils with magic-angle spinning, dynamic nuclear polarization NMR. *J. Am. Chem. Soc.* **2011**, *133*, 13967–13974.

35 Kiesewetter, M.; Corzilius, B.; Smith, A. A.; Griffin, R. G.; Swager, T. M. Dynamic Nuclear Polarization with a Water-soluble Rigid Biradical. *J. Am. Chem. Soc.* **2012**, *134*, 4537–4540.

36 Rosay, M.; Weis, V.; Kreischer, K. E.; Temkin, R. J.; Griffin, R. G. Two-dimensional $^{13}C$-$^{13}C$ correlation spectroscopy with magic angle spinning and dynamic nuclear polarization. *J. Am. Chem. Soc.* **2002**, *124*, 3214–3215.

37 Akbey, Ü.; Franks, W. T.; Linden, A.; Lange, S.; Griffin, R. G.; Rossum, B.-J. v.; Oschkinat, H. Dynamic Nuclear Polarization of Deuterated Proteins. *Angew. Chem., Int. Ed.* **2010**, *49*, 7803–7806.

38 Harbison, G. S.; Herzfeld, J.; Griffin, R. G. Solid-State $^{15}N$ Nuclear Magnetic-Resonance Study of the Schiff-Base in Bacteriorhodopsin. *Biochemistry* **1983**, *22*, 1–5.

39 Harbison, G. S.; Smith, S. O.; Pardoen, J. A.; Courtin, J. M. L.; Lugtenburg, J.; Herzfeld, J.; Mathies, R. A.; Griffin, R. G. Solid-State C-13 Nmr Detection of a Perturbed 6-S-Trans Chromophore in Bacteriorhodopsin. *Biochemistry* **1985**, *24*, 6955–6962.

40 Jaroniec, C. P.; Filip, C.; Griffin, R. G. 3D TEDOR NMR experiments for the simultaneous measurement of multiple carbon-nitrogen distances in uniformly C-13, N-15-labeled solids. *J. Am. Chem. Soc.* **2002**, *124*, 10728–10742.

41 Michaelis, V. K.; Markhasin, E.; Daviso, E.; Herzfeld, J.; Griffin, R. G. Dynamic Nuclear Polarization of Oxygen-17. *J. Phys. Chem. Lett.* **2012**, *3*, 2030–2034.

42 Vitzthum, V.; Mieville, P.; Carnevale, D.; Caporini, M. A.; Gajan, D.; Cope, C.; Lelli, M.; Zagdoun, A.; Rossini, A. J.; Lesage, A.; Emsley, L.; Bodenhausen, G. Dynamic nuclear polarization of quadrupolar nuclei using cross polarization from protons: surface-enhanced aluminium-27 NMR. *Chem. Commun.* **2012**, *48*, 1988–1990.